Spatiotemporal Relationships Between the Cell Shape and the Actomyosin Cortex of Periodically Protruding Cells

Meghan K. Driscoll,[1] Wolfgang Losert,[1,2] Ken Jacobson,[3,4] and Maryna Kapustina[3]*

[1]Department of Physics, University of Maryland, College Park, Maryland
[2]Institute for Physical Science and Technology, University of Maryland, College Park, Maryland
[3]Department of Cell Biology and Physiology, School of Medicine, UNC Chapel Hill, North Carolina
[4]Lineberger Comprehensive Cancer Center, School of Medicine, UNC Chapel Hill, North Carolina

We investigate the dynamics of cell shape and analyze the actin and myosin distributions of cells exhibiting cortical density traveling waves. These waves propagate by repeated cycles of cortical compression (folding) and dilation (unfolding) that lead to periodic protrusions (oscillations) of the cell boundary. The focus of our detailed analysis is the remarkable periodicity of this phenotype, in which both the overall shape transformation and distribution of actomyosin density are repeated from cycle to cycle even though the characteristics of the shape transformation vary significantly for different regions of the cell. We show, using correlation analysis, that during traveling wave propagation cortical actin and plasma membrane densities are tightly coupled at each point along the cell periphery. We also demonstrate that the major protrusion appears at the wave trailing edge just after the actin cortex density has reached a maximum. Making use of the extraordinary periodicity, we employ latrunculin to demonstrate that sequestering actin monomers can have two distinct effects: low latrunculin concentrations can trigger and enhance traveling waves but higher concentrations of this drug retard the waves. The fundamental mechanism underlying this periodically protruding phenotype, involving folding and unfolding of the cortex-membrane couple, is likely to hold important clues for diverse phenomena including cell division and amoeboid-type migration. © 2015 The Authors. Cytoskeleton Published by Wiley Periodicals, Inc.

Key Words: actin cortex; traveling wave; cell shape; correlation analysis; amoeboid-type migration

*Address correspondence to: Maryna Kapustina, Department of Cell Biology and Physiology, School of Medicine, UNC Chapel Hill, NC, USA. E-mail: mkapust@med.unc.edu
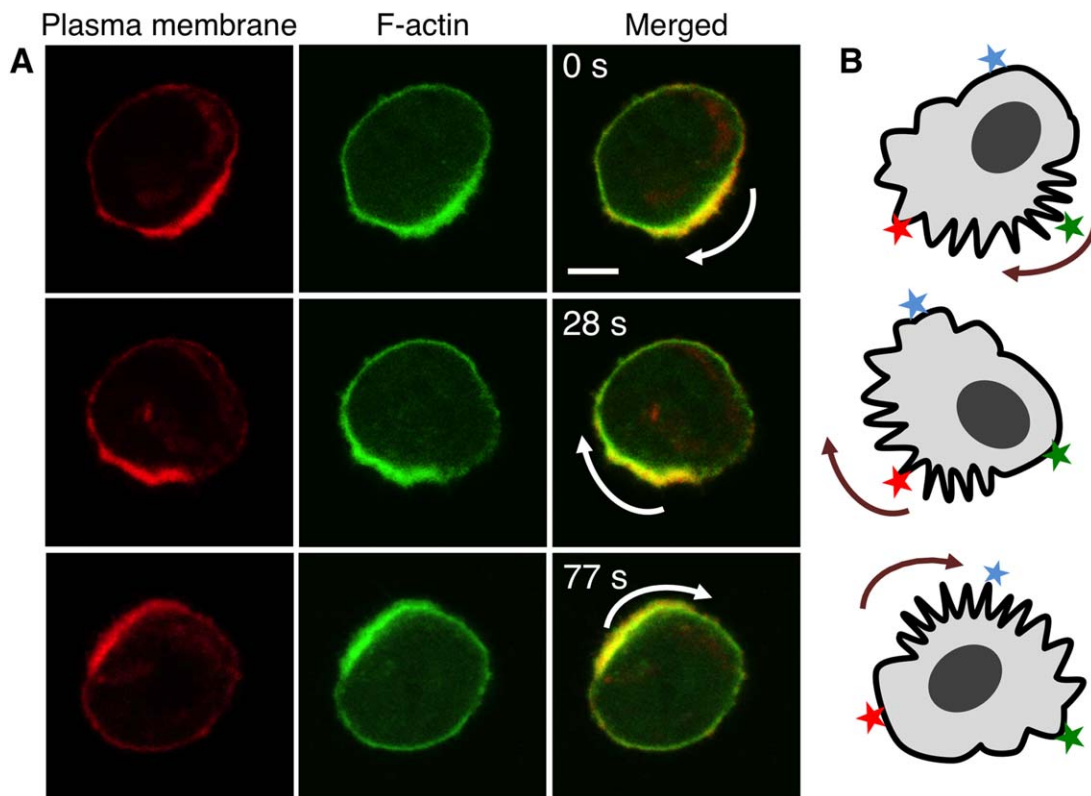
Introduction

The actin cytoskeleton, a complex network of dynamically polymerizing and depolymerizing filaments, is the prime determinant of local and global cell shape. This network of actin filaments responds with rapid changes in organization and dynamics to a variety of stimuli and therefore has a unique role in major cell functions including migration, cytokinesis, differentiation, and environmental adaptation. While a single actin filament is semi-flexible, a group of filaments can form more stable and rigid structures by incorporation of specific actin-binding proteins [Tseng et al., 2001; Gardel et al., 2004; Revenu et al., 2004; Kasza et al., 2009; Courson and Rock, 2010]. The actin dynamics involved in cell shape changes and migration on flat substrates have been well characterized by intensive research over the past several decades [Mitchison and Cramer, 1996; Rottner and Stradal, 2011; Blanchoin et al., 2014]. Two main mechanisms have been demonstrated to generate the forces needed to drive deformation of cells: actin polymerization and myosin contraction. Actin polymerization alone was found to generate sufficient forces to drive protrusions at the leading edge of migrating cells in, for example, fibroblasts and keratocytes [Mitchison and Cramer, 1996; Prass et al., 2006; Keren et al., 2008; Rottner and Stradal, 2011]. Myosin contraction is known to be essential for most types of cell migration and shape transformations [Maciver, 1996; Keren et al., 2008; Cai et al., 2010; Kasza and Zallen, 2011;]. While both mechanisms can exist at the same time and be connected to each other through the actomyosin network, in the contexts of mesenchymal and amoeboid migration, one of these mechanisms usually dominates. Here we analyze the actomyosin network

Fig. 1. Compression-dilation waves in periodically protruding cells. (**A**) Fluorescence images of plasma membrane marker (red) and Lifeact, an F-actin marker, (green) during periodic protrusions of a rounded CHO cell. This time series shows a traveling wave of membrane–cortex fluorescence intensity around the cell border, with arrows indicating the direction of travelling wave propagation. (**B**) A cartoon showing a cell with membrane-cortical folds on the periphery. The cyclic process of folding-unfolding creates a traveling wave. The colored stars represent three fiduciary marks on the periphery. These marks remain approximately stationary when the wave of cortical contraction travels through the position of the fiduciary marks, indicating that cortical material is not transported laterally around the periphery. [Color figure can be viewed in the online issue, which is available at wileyonlinelibrary.com.]

dynamics and corresponding cell deformations during periodic, morphological oscillations in rounded cells. Such analysis can provide key insights into the functioning of the dynamic, spatially heterogeneous actomyosin cortex that underlies cell shape changes in phenomena as diverse as cell division and amoeboid-type migration.

In our previous work [Kapustina et al., 2013] we suggested that the compression (folding) and dilation (unfolding) of the coupled plasma membrane–actin cortex layer may be used as a general mechanism for rapid transformations of rounded cells. We investigated the periodic protrusions that can be exhibited spontaneously by many cells following rapid detachment from a substrate. These periodic morphological changes (oscillations) can be induced or further enhanced by microtubule depolymerization. We demonstrated that periodic protrusions are the result of compression (cortical folding) and subsequent dilation (cortical unfolding) of the plasma membrane–cortex layer and suggested that the repeated compression–dilation cycles are responsible for a traveling wave of plasma membrane–cortical actin density around the cell boundary.

An example of a traveling wave in plasma membrane and actin density in an oscillating cell is shown in Fig. 1 and Supporting Information Movie 1. We assume that the fluorescence intensity is proportional to the number of fluorescently labeled molecules and thus provides a reliable estimate of relative density. It is important to note that the wave motion does not represent actual transport of material around the periphery, but rather is due to compression and dilation of the membrane–cortex couple as illustrated by the cartoon in Fig. 1B. The propagating wave of cortex density is likely to be only sustainable in cells with rounded morphology, where the available plasma membrane area is greater than is required to contain the cell volume [Kapustina et al., 2013].

Previously we used Fourier analysis of the trajectory of the cell center of mass to analyze the oscillatory motion [Costigliola et al., 2010]. However, those global analyses did not provide us with detailed information about the traveling wave, the periodic location of the protrusion-retraction events, or about the correlation between the density of the cortical actin traveling wave and associated myosin, and the dynamic shape changes. Therefore, in this article, we employed a quantitative approach based on the analysis of the signal from different fluorescence markers to elucidate the timing of traveling wave propagation and the corresponding shape transformation.

Our findings highlight novel details of the natural wave behavior and its response to perturbations, and provide crucial information for mechanistic theoretical models: We demonstrate that the density of plasma membrane and actin cortex are highly recurrent in time and cross-correlated with each other. We find that the predominant protrusion occurs at the trailing edge of traveling waves. We further find that cortex myosin density is highly organized spatiotemporally, and that it correlates tightly with the density of cortical F-actin with an apparent small delay. Because the cell morphological oscillations exhibit extremely stable spatiotemporal patterns, the waves provide an excellent model to study the response of the actomyosin cortex to perturbations. To demonstrate this, we analyzed the effect of sequestration of actin monomers by latrunculin treatment, finding that sequestration of actin monomers may be used to trigger the onset of waves, and to tune the wave speed.

Results

Metrics of Cell Shape and Shape Dynamics

To investigate the dynamics of cell morphological transformations, we previously developed a set of metrics to characterize rapidly changing cell shapes [Driscoll et al., 2011]. Here we apply these metrics, along with correlation analysis, to interrogate the periodic protrusive phenotype. We observe this phenotype in CHO cells that were stably transfected with Lifeact-GFP, a small peptide that has been widely exploited to visualize F-actin [Riedl et al., 2008]. Time series of fluorescence images of periodically protruding CHO cells were recorded using a laser scanning confocal microscope. Compression-dilation waves can travel around the cell periphery in any direction in 3D space which can cause some trajectories to transiently disappear from the confocal plane. To simplify the interpretation of the shape dynamics, we selected for analysis only cells where the compression-dilation wave travels on a plane nearly coincident with the focal plane.

The cell boundary was extracted and tracked using an active contour based algorithm. Mathematically, the cell boundary in each frame was represented as a sequence of equidistant points along the boundary (Fig. 2A). In each frame, boundary point 0 was defined as the boundary point that was closest to zero degrees relative to the cell center (calculated as the average position of all boundary points) (Fig. 2B). The remaining boundary points were sequentially labeled in the counter-clockwise direction (Supporting Information Movie 2).

As a metric of cell shape, we used boundary radius, which accentuates global features of cell shape such as the periodic protrusions [Driscoll et al., 2011]. We defined the cell radius at each boundary point as the distance from that boundary point to the cell center. In Fig. 2C, the boundary radius, represented by color, is shown for a cell in a single

frame. The boundary points with the greatest radius, which are farthest from the cell center, are shown as red, whereas boundary points with the smallest radius, which are closest to the cell center, are shown as blue. For improved visualization and time sequence analysis, we represented the radius as a single vertical strip by cutting the boundary at boundary point 0 then stretching it taut while preserving the color coding (Fig. 2D).

We also investigated the possibility of using boundary curvature as a metric of cell shape (Supporting Information Fig. S1). However, boundary curvature is most responsive to small, local features in the boundary, and in the current investigation we are primarily interested in the compression-dilation wave, which is a large, global feature of cell shape. We therefore here primarily use boundary radius rather than boundary curvature.

As a metric of cell shape dynamics, we measured the local boundary speed at each boundary point using the boundary positions in consecutive frames. Figure 2E shows the boundary motion of a representative cell. The boundary position in frame t is shown as a black line, and its position in frame $t+1$ is shown as a gray line. The blue lines represent boundary regions that are moving inwards (toward the cell body), whereas the red lines represent boundary regions that are moving outwards (away from the cell body). The boundary motion is defined as the change in position of the boundary in a direction approximately normal to the original boundary, and in Fig. 2E is proportional to the length of the colored lines. As we did with boundary radius, we also represented boundary motion as a colored vertical stripe (Fig. 2F).

Radius and Boundary Motion Are Highly Structured

To investigate how the radius and boundary motion vary in time, we measured the value of the metrics at each boundary point and in each frame or frame pair (Supporting Information Movies 3 and 4). Next we tracked the boundary points from frame to frame by associating same-labeled boundary points in successive frames. The kymographs in Figs. 3A and 3B show how the radius and boundary motion vary both in time and along the boundary. (Similar kymographs for two other cells are shown in Supporting Information Fig. S2). In these kymographs each vertical line represents the information from one frame (as exemplified by the stripes in Figs. 2D and 2F), and each horizontal line represents the behavior of one boundary point as a function of time.

Examining the kymographs, we observe multiple layers of structure indicative of the reproducible and repetitive nature of the morphological oscillations. Consistent with prior observations of periodic protrusions, both kymographs (Figs. 3A and 3B) show that a wave, apparent as repeated tilted lines in the kymographs, propagates laterally around the cell periphery. From the motion metric (Fig. 3B) we observe that a wave of high outwards boundary
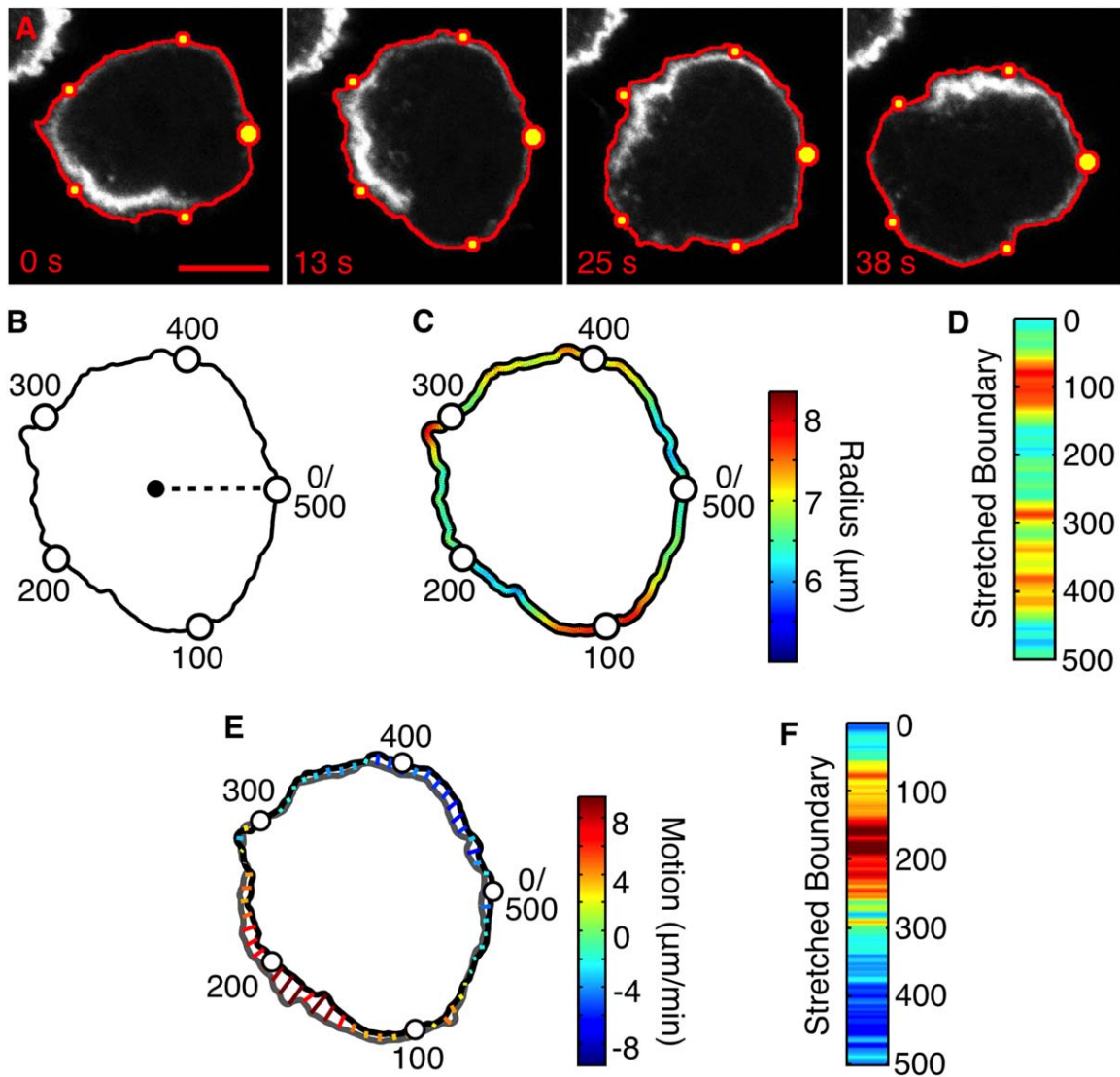
Fig. 2. Metrics for boundary shape and motion of a periodically protruding CHO cell. (**A**) A fluorescence image sequence of a cell with labeled actin (Lifeact-GFP). The cell boundary, which is represented by 500 boundary points, is overlaid in red with every 100th boundary point indicated by a yellow dot. The 0th boundary point is indicated by the largest dot. The scale bar is 5 μm. (**B**) For each boundary point in each frame, we measured the radius, which is defined as the distance from the cell centroid to each boundary point. Here the radius at the 0th boundary point is represented by the dashed line. (**C**) The cell boundary colored by radius. The farthest boundary regions from the cell centroid are colored red, whereas the closest boundary regions are colored blue. (**D**) The cell radius shown represented by a single colored line. This is equivalent to cutting the colored boundary shown in C at the 0th boundary point, pulling it taut, and arranging it vertically. (**E**) The boundary motion between the frame at 0 sec, shown as a solid black line, and the frame at 16 s, shown as a dashed black line. Each boundary point in the earlier frame is tracked to a boundary point in the later frame. Protrusions are represented as red lines, whereas retractions are represented as blue lines. (**F**) The boundary motion represented by a single line. [Color figure can be viewed in the online issue, which is available at wileyonlinelibrary.com.]

speed propagates around the cell; this motion wave appears as tilted red streaks. From the shape metric (Fig. 3A), we observe that a more diffuse wave of increasing radius propagates around the cell; this shape wave is most easily observed as either a wave of low radius (tilted blue streaks) or high radius (tilted red streaks).

Notice that while a wave clearly propagates around the boundary, it does not do so uniformly. While the system is repetitive in time, it is not uniform in space. As can be seen from the radius kymograph (Fig. 3A), some boundary regions greatly extend outwards reproducibly and repetitively (e.g., near boundary point 250), whereas other boundary regions only slightly extend outwards (e.g., near boundary point 150). Furthermore, from Fig. 3B we see that the protrusion speed also varies within the wave—in this example it is larger near boundary point 100 at 0 min (dark red color code) than near boundary point 300 at 1 min (yellow-blue color code). Given the spatial inhomogeneity in the amount and speed of protrusion, it is quite surprising that for any given boundary point these
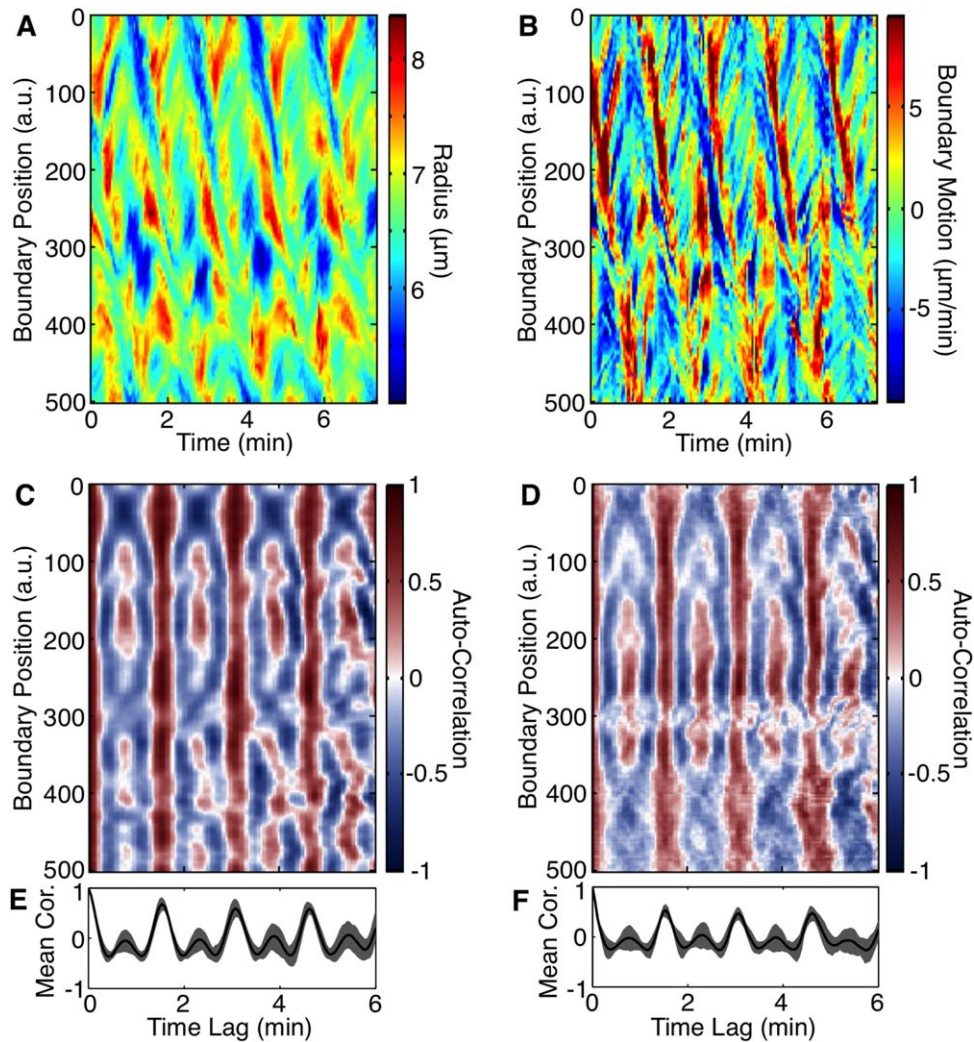
Fig. 3. The shape and motion of periodically protruding CHO cells are highly structured. (**A**) The boundary radius of a cell as a function of boundary position and time. Each vertical slice represents the radius of the entire boundary in one frame, whereas each horizontal slice represents the radius of a single boundary point as a function of time. The regions farthest from the cell center appear red, whereas the regions closest appear blue. (**B**) The boundary motion of the same cell. Protruding regions appear red, retracting regions appear blue, and stationary regions appear green. (**C**) The auto-correlation of the cell's boundary radius. Each horizontal line shows the auto-correlation at the specified boundary point. Large positive correlations appear red, large negative correlations appear blue, and regions of zero correlation appear white. (**D**) The auto-correlation of the cell's boundary motion. (**E**) The mean auto-correlation of boundary radius averaged across all boundary points. The lower boundary of the gray shaded region indicates the 25th percentile of correlations at each time lag, whereas the upper boundary of the gray shaded region indicates the 75th percentile of the correlations. (**F**) The mean auto-correlation of boundary motion averaged across all boundary points. The lower boundary of the gray shaded region indicates the 25th percentile of correlations at each time lag, whereas the upper boundary of the gray shaded region indicates the 75th percentile of the correlations.

metrics are very reproducible and periodic. Notable features in the kymograph appear at approximately the same position on the boundary during each period. For example, a blue region appears near boundary point 300 every ∼90 s, as can be seen in Fig. 3A. Therefore, we conclude that each region of the boundary has a different responsiveness to the wave, yet the response is highly reproducible in time.

To quantify both the reproducibility in time and the spatial heterogeneity, we calculated the auto-correlation of radius and boundary motion separately for each boundary point. The autocorrelation provides a measure of how these

values (radius or boundary motion) change with time delay τ. For example, when considering the autocorrelation of radius, a value of 1 indicates that the radius is the same for all pairs of frames separated by a time delay τ, a value of 0 indicates no statistically significant relationship, and a value of −1 indicates that a large radius is likely to be followed by a small radius a time τ later (or vice versa). First, we determined the autocorrelations for each boundary point separately for radius and boundary motion as shown in Figs. 3C and 3D, respectively. The periodic long vertical red stripes demonstrate high autocorrelation which is the result of the traveling wave moving around the cell with
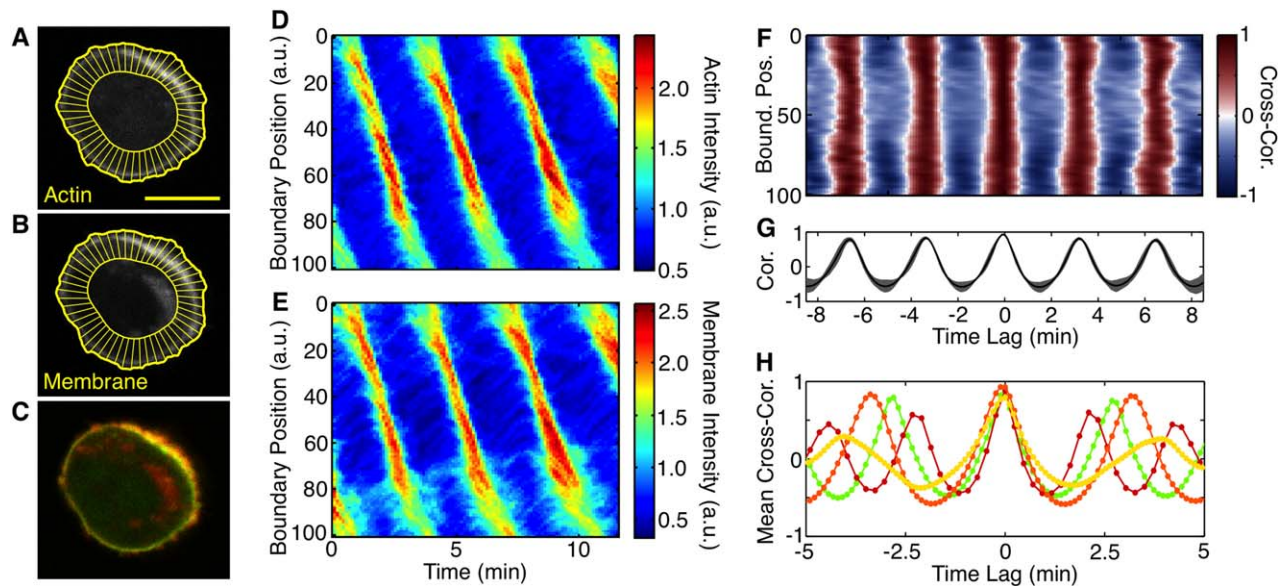
Fig. 4. The plasma membrane and actin intensities are highly periodic and cross-correlated. (**A**) A fluorescence image of labeled actin (Lifeact-GFP). The region near the cell boundary is tiled by virtual windows, shown in red, and the mean actin intensity is measured in each window. (Note that the actual number of windows used for calculations is twice that shown.) (**B**) A fluorescence image of a dually acylated membrane-bound reporter conjugated to RFP that inserts into the inner leaflet of the plasma membrane. The region near the cell boundary is tiled by the same windows as in A. Scale bars in A and B are 10 μm. (**C**) The merged actin (green) and membrane (red) fluorescence images. (**D**) Kymograph of membrane fluorescence near the boundary as a function of boundary position and time. Boundary regions with high membrane intensity appear red, whereas regions with low intensity appear blue. (**E**) Kymograph of cortical actin fluorescence near the boundary as a function of boundary position and time. (**F**) The cross-correlation of actin and membrane intensities. Each horizontal line shows the cross-correlation at the specified boundary point. Regions of large positive correlation appear red, regions of large negative correlation appear blue, and regions of zero correlation appear white. (**G**) The mean actin-membrane intensity cross-correlation averaged across all of the boundary points. At each time lag, the gray bar indicates the 25th to the 75th percentile of auto-correlation values measured across boundary positions. (H) The mean actin-membrane cross-correlation, averaged over boundary position, for four cells, each shown in a different color.

nearly constant speed. The distance between strips on the time lag axis provides the period of the traveling wave. The short red stripes that appear between the long stripes indicate that different regions of the boundary exhibit specific periodic features in addition to the main wave. For example, boundary point 250 in Fig. 3D shows a motion wave with roughly double the frequency as the motion wave at boundary point 400. The auto-correlation averaged across all boundary points is further shown in Figs. 3E and 3F. The auto-correlations confirm that the shape and shape dynamics at each boundary point are highly periodic, even though the wave propagates non-uniformly around the cell.

Cortical Actin Dynamics Are Highly Periodic

We next examined the temporal periodicity of cortical actin by tiling the region near the cell boundary and measuring the mean actin intensity in each tile. Figure 4A shows an example tiling overlaid on a fluorescence image of Lifeact-GFP. We constructed a kymograph of actin intensity as we did for the boundary radius and motion measures (Fig. 4D). Similar to the shape and shape dynamics metrics, we find that a wave of high actin intensity propagates about the cell boundary. This wave is visible in Fig. 4D as tilted, thick red lines.

Because actin intensity is more regular than boundary radius or motion, we used actin intensity to characterize the heterogeneity of the wave period across cells and within individual cells. We measured the wave period as the delay time of the first peak in the actin intensity auto-correlation. Supporting Information Fig. S3E shows the actin intensity auto-correlations for ten cells. We found a mean wave period of 2.1 min with a standard deviation of 0.3 min. While the autocorrelation of a perfectly periodic system would be one, measurement uncertainties as well as variations in wave period and amplitude all reduce the autocorrelation. For 10 cells the mean correlation at one period is 0.72 with a standard deviation of 0.13 but for some cells the autocorrelation peak reaches very high values of ∼0.9. As with the radius and motion measures, while the main wave propagates non-uniformly around the cell, the behavior at each boundary point is very periodic (Supporting Information Fig. S3).

Actin and Membrane Intensities Are Highly Correlated

To examine the relationship between cortical actin and the plasma membrane, we simultaneously expressed plasma membrane tracker (RFP) and Lifeact (GFP). As

mentioned above, Fig. 4A shows a Lifeact fluorescence image overlaid by the tiles used to calculate intensity along the boundary, Fig. 4B shows a plasma membrane fluorescence image overlaid by the same tiles, and Fig. 4C shows a composite of the two fluorescence images. Comparing the actin intensity (Fig. 4D) and plasma membrane intensity kymographs (Fig. 4E), we find by inspection that they are quite similar. (Here, we measured the cell boundary position from the plasma membrane channel.) While both kymographs show waves that propagate non-uniformly along the boundary with varying magnitude, the two waves have similar intensities everywhere along the boundary. This indicates that the folding/unfolding events giving rise to intensity changes are similar in both channels.

To further compare the actin and membrane intensities, we cross-correlated the two signals. Figure 4F shows the cross-correlation at every boundary point for the cell shown in the previous panels, Fig. 4G shows the cross-correlation averaged across boundary points for this cell, and Fig. 4H shows the cross-correlation for multiple cells. As expected, the actin and membrane intensities are highly correlated. This correlation supports the idea that in the compression/dilation traveling wave the actin cortex and plasma membrane are tightly coupled.

Actin Intensity, Shape, and Motion Are Temporally Stereotyped

In our previous work we suggested that cortical travelling waves result from the cyclic folding and unfolding of the membrane and cortex, as illustrated schematically in Fig. 1 (right). By investigating the boundary radius, boundary motion and cortical actin distribution, we determined that all three exhibit traveling waves. To understand how these three measured waves temporally interrelate as part of one physical wave, we investigated the cross-correlations between cortical actin, cell shape, and boundary movement.

Figure 5A shows fluorescence images of a cell expressing Lifeact-GFP with the extracted boundary overlaid for two successive frames. Protrusive boundary regions are colored red, whereas retractive regions are colored blue. Notice that regions of high actin intensity (blue arrow) appear to precede regions of protrusive motion (red arrow). From the actin intensity (Fig. 5B) and boundary motion (Fig. 5C) kymographs we see that indeed the wave of high actin intensity precedes the wave of protrusive motion. This becomes evident when superimposing the location of peak actin intensity from Fig. 5B (dashed black line) onto the kymograph of boundary motion. The dashed black line appears slightly behind the wave of protrusive motion indicating that protrusions develop on the trailing edge of the F-actin density wave just after the cortex density has reached a maximum.

To determine the delay between actin intensity and protrusive motion, we measured the cross-correlation between the two measures. The position of cross-correlation peak relative to zero time lag determines how two cross-correlated functions relate in time. Figure 5D, shows the cross-correlation between cortical actin and boundary protrusive motion averaged across all boundary points. The peak of this cross-correlation (arrow) is located slightly before time lag zero which indicates that high actin intensity precedes protrusive movement. For the ten cells analyzed, cortical actin precedes protrusive movement by an average of 15.5 s with a standard deviation of 3.2 s (Fig. 5F). The situation is opposite for retractive movement with high actin intensity lagging retractive movement. Figure 5E shows the averaged actin-retractive motion cross-correlation with an arrow indicating the peak. We further confirmed these observations by cross-correlating actin intensity with boundary radius. Figure 5G shows that actin intensity is negatively correlated with boundary radius.

Actin and Myosin Intensities Are Highly Correlated

Our previous work established that myosin II was intimately associated with the cortical actin traveling wave. We therefore quantitatively examined the spatiotemporal relationship between actin and myosin II. To accomplish this, Lifeact-GFP and myosin-RFP were simultaneously expressed in the same cells (Figs. 6A–6C). The cortical actin (Fig. 6D) and myosin (Fig. 6E) intensity kymographs are similar, as quantified in the myosin-actin intensity cross-correlation shown in Fig. 6F. Figure 6G shows the myosin-actin cross-correlations averaged across all boundary points for 10 cells. In Figs. 6F and 6G, the high cross-correlation at a time lag of 0 min indicates that the myosin and actin intensities vary similarly over time. However, in these panels, the peak cross-correlation is slightly offset from 0 minutes. To better detect this offset, we measured the myosin-actin cross-correlation in cells imaged at a much higher frame rate (Fig. 6H) using spinning disk confocal microscopy. For the seven cells shown in Fig. 6H myosin is delayed with respect to cortical actin by a mean of 1.3 ± 0.3 seconds (SEM) but with considerable variability across cells. Both Lifeact-GFP/myosin-RFP and Lifeact-RFP/myosin-GFP expressing cells show a delay in myosin. A plausible explanation for this delay is that myosin II accumulation temporally lags actin accumulation with the wave. Alternatively, the measured temporal delay could be generated by a spatial asymmetry within the traveling wave, for example actin and myosin could have distinct spatial distributions with myosin on average slightly closer to the cell center than actin. Thus, we conclude that actin and myosin have a very similar spatiotemporal distribution though the appearance of myosin may be slightly delayed or offset from actin in the cortical traveling wave.
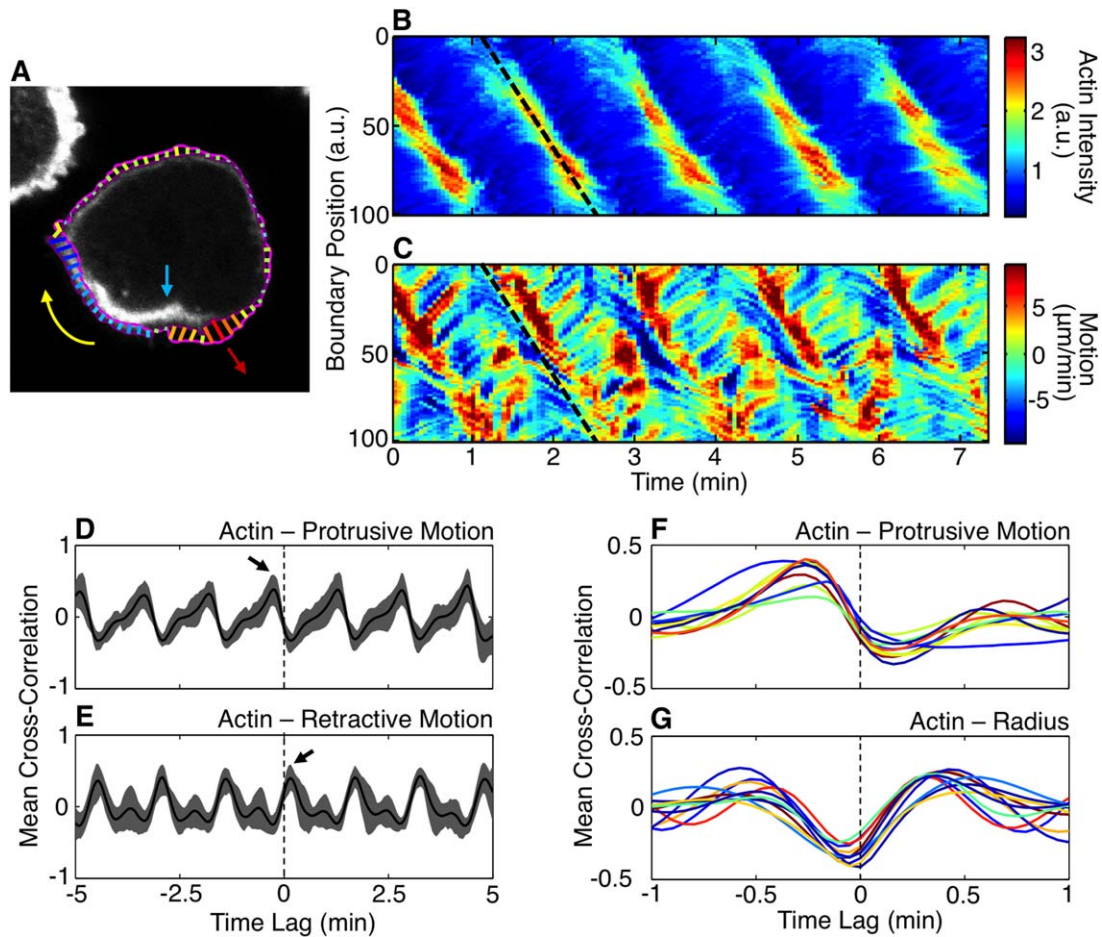
Fig. 5. Temporal ordering of the compression-dilation wave. (**A**) A fluorescence image of labeled actin (Lifeact-GFP). The direction of the propagating wave is indicated by the yellow arrow. The boundary motion measure between two consecutive frames ($t = 3s$) is overlaid with red lines indicating regions of protrusive motion and blue lines indicating regions of retractive motion. The red arrow shows the direction of the major protrusion that appears at the end of the actin wave and the blue arrow indicates the highest actin density. (**B**) Actin fluorescence intensity of the same cell shown as a function of boundary position and time. (**C**) The boundary motion of the same cell as a function of boundary position and time. (**D**) The actin-protrusive motion cross-correlation, averaged across boundary position, for the same cell. High actin intensity precedes large protrusive motion (see black arrow showing that peak comes slightly before 0 time lag). (**E**) The actin-retractive motion cross-correlation, averaged across boundary position, for the same cell showing that actin density somewhat lags retraction. (**F**) The actin-protrusive motion cross-correlation, averaged across boundary position, for 10 cells. (**G**) The actin-radius cross-correlation, averaged across boundary position, for 10 cells. Actin intensity and cell radius are negatively correlated. [Color figure can be viewed in the online issue, which is available at wileyonlinelibrary.com.]

In Addition to the Main Wave, There Are Backward-directed Waves

Examining the motion kymographs more closely (e.g., Fig. 5C), we noticed that there are additional short red streaks which are connected to the main wave but tilted in the opposite direction. To study the nature of these waves we analyzed boundary curvature, since this metric allows facile recognition of smaller features. Figure 7A shows an enlarged section of the actin intensity kymograph from Figs. 6D and 7B shows the corresponding kymograph of boundary curvature. Overlaying the location of the actin intensity wave (dashed black line) on boundary curvature, we see that there are indeed waves of high boundary curvature (for example the tilted red line between the stars on Fig. 7B) that propagate counter to the main compression-dilation wave and that are not readily visible in the actin intensity kymograph. The time series in Fig. 7C (also Supporting Information Movie 5), shows the traveling of this small curved boundary region, indicated by the arrowheads, along the cell boundary from position 460 to position 385 within 25 s. Like other features of cell shape in the periodically protruding phenotype, these counter-propagating short-duration waves reproducibly occur at the same boundary positions over multiple wave periods (see for example the boundary curvature kymograph in Supporting Information Fig.
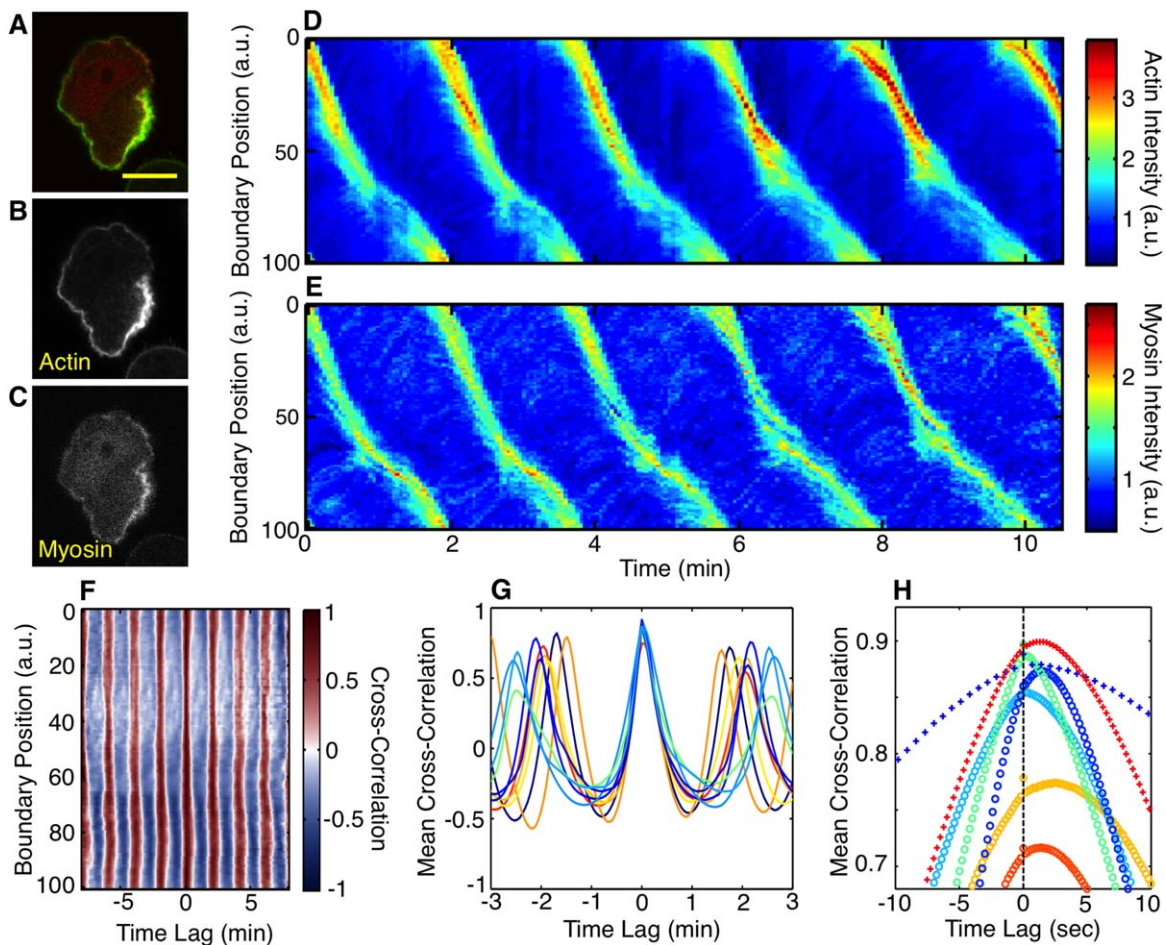
Fig. 6. Actin and myosin intensities are highly cross-correlated. (**A**) A two-color fluorescence image of an actin (Lifeact-GFP) in green and myosin labeled cell (MLC-RFP) in red. Scale bar indicates 10 µm. (**B**) and (**C**) show the actin and myosin channels separately. Kymographs representing (**D**) actin and (**E**) myosin fluorescence intensities at the cell boundary as a function of boundary position and time. (**F**) The myosin-actin cross-correlation of the same cell. Each horizontal line shows the cross-correlation at the specified boundary point. Regions of large positive correlation appear red, regions of large negative correlation appear blue, and regions of zero correlation appear white. (**G**) The myosin-actin intensity cross-correlations, averaged across boundary points, for 10 cells. (**H**) Myosin-actin intensity cross-correlations measured from cells imaged at high temporal resolution. Circles are cross-correlations measured from myosin-RFP and actin-GFP labeled data, whereas pluses are cross-correlations measured from myosin-GFP and actin-RFP labeled data. [Color figure can be viewed in the online issue, which is available at wileyonlinelibrary.com.]

S1C). Such waves are a natural consequence of the cell surface distortions/compression following the massive protrusion that occurs at the trailing edge of the cortical actin traveling wave. Without kymographic analysis, such features would have been difficult to recognize from an image series alone.

Latrunculin Treatment Has Two Distinct Effects

Because the dynamics of the periodic protrusive phenotype without perturbation are so regular and reproducible in terms of the periodic folding and unfolding of the actin cortex, this system is ideally suited for measuring the dynamic response of the cell to drugs and other perturbations. Specifically, for each boundary point, the dynamics of protrusion, retraction, and actin and myosin intensities can be predicted with great accuracy as evident from the strong time correlations. This allows us to measure pertur-

bations of the dynamics in a completely novel way. To illustrate this idea we used latrunculin to sequester actin monomers and analyze how this affects cortical actin dynamics and boundary motion for each point along the periphery and for the entire cell.

The experiment consisted of five different episodes of four cumulative latrunculin treatments with the following concentrations: 60, 60, 120, and 240 nM so that in the last phase of the experiment 480 nM latrunculin was present. After the addition of each single latruculin dose cells were permitted to equilibrate for at least 35 min. Supporting Information Movie 6 presents a time-lapse recording of merged DIC and actin intensity images for representative sequences of each episode.

Analyzing the images, we found that treatment with lower concentrations of latrunculin (<120 nM) enhances and can even initiate periodic protrusions. Figure 8 shows
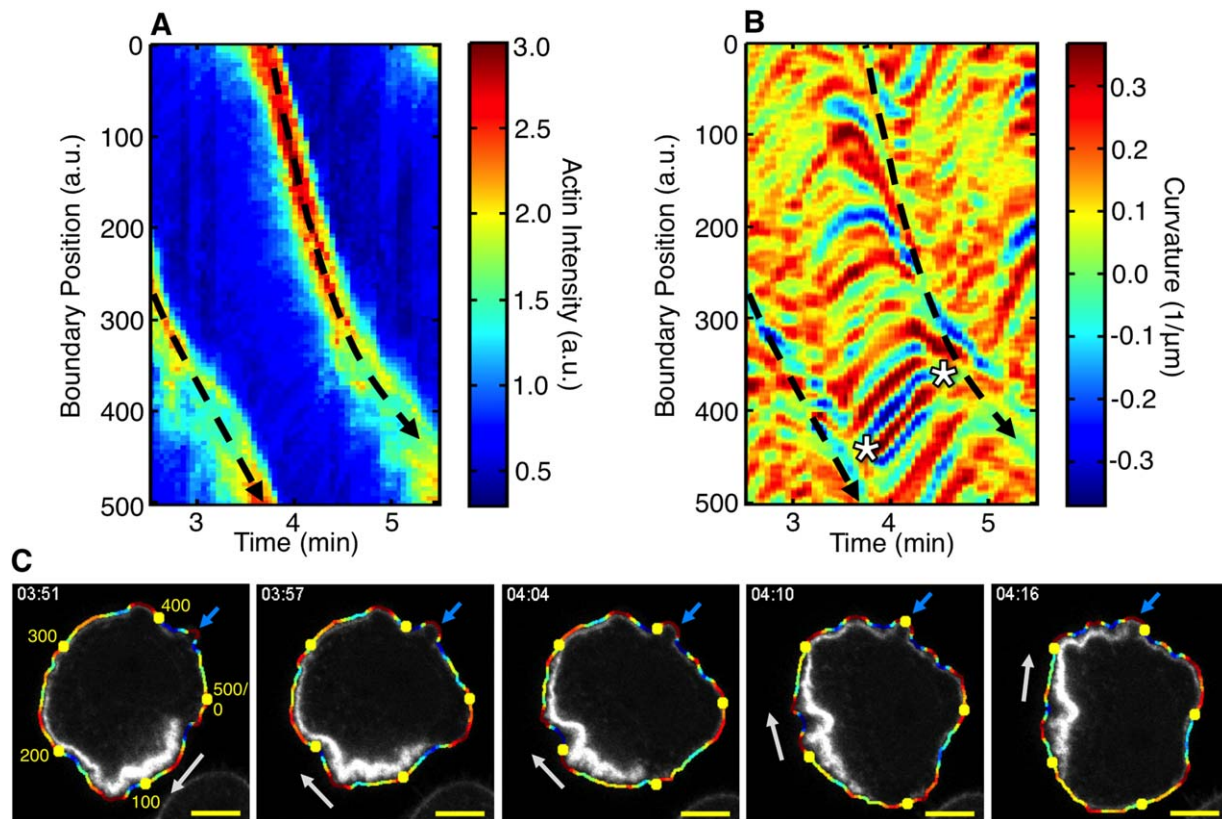
Fig. 7. Waves of boundary curvature propagate laterally in the direction opposite to the main compression-dilation wave. (**A**) Cortical actin fluorescence intensity as a function of boundary position and time. The black dashed lines with arrows show the position of the main wave traveling in the clockwise direction. (**B**) Boundary curvature as a function of boundary position and time. Notice that there are many short waves of high boundary curvature (red stripes on the kymograph) that propagate opposite to the direction of the actin fluorescence intensity wave, marked by black lines. The trajectory of one representative backward directed (counter clockwise) wave marked by two stars and the corresponding image series is shown in **C**. (**C**) The time series of F-actin fluorescence images showing traveling wave of cortical actin density. The white arrows show the direction (clockwise) of wave propagation. By contrast, a wave of boundary curvature that travels counter clockwise can be seen on the cell boundary. At time $t = 3.5$, a small, highly curved feature appears near boundary position ~460 (blue arrowhead) and starts moving along the cell periphery in the direction opposite to the main compression-dilation wave. By $t = 4.2$, this small, highly curved feature reaches boundary position ~385. Times are in minutes and seconds. [Color figure can be viewed in the online issue, which is available at wileyonlinelibrary.com.]

the kymographs of actin intensity (Fig. 8A) and boundary movement (Fig. 8B) for one cell during the experiment. (Note that the tilts in the kymographs are not as obvious because the time scale is highly compressed.) The initiation and enhancement of the traveling wave occurs after a lag time; since the strong periodicity of the cortical actin wave appears only after some delay following the first latrunculin treatment (episodes #1 & #2). Small doses also increase the protrusion and retraction speed, which is indicated by the increasing presence of dark red and dark blue colors on the motion kymograph after the first two doses of latrunculin (episodes #2 and #3). After further additions of 120 and 240 nM, latrunculin tends to reduce the protrusion and retraction speeds (episode #4), which is manifested by the disappearance of red and blue color from the periodic stripes in the motion kymograph; eventually the wave becomes disorganized and finally halts as seen by the lack of periodicity and the lack of motion at the end of episode #5. This drastic effect is preceded by the gradual increase in

period seen after subsequent additions of 60 and 120 nM latrunculin (Fig. 8C). The decreasing spatial frequency of stripes on the kymograph for episode #4 clearly demonstrates this effect but the gradual slowdown of the traveling wave during episode #3 is hard to distinguish and can be only determined via careful measurement (see Materials and Methods).

Discussion

A laterally propagating compression/dilation wave of the coupled actin cortex and plasma membrane is the major feature of the periodic protrusive phenotype. This wave, first discovered in [Kapustina et al., 2013], and the associated cell morphological behavior [Pletjushkina et al., 2001; Costigliola et al., 2010] has many similarities to the blebby type of amoeboid migration. Thus, for example both phenotypes exhibit rounded protrusions, low adhesion and strong dependence on RhoA activation [Friedl and Wolf,
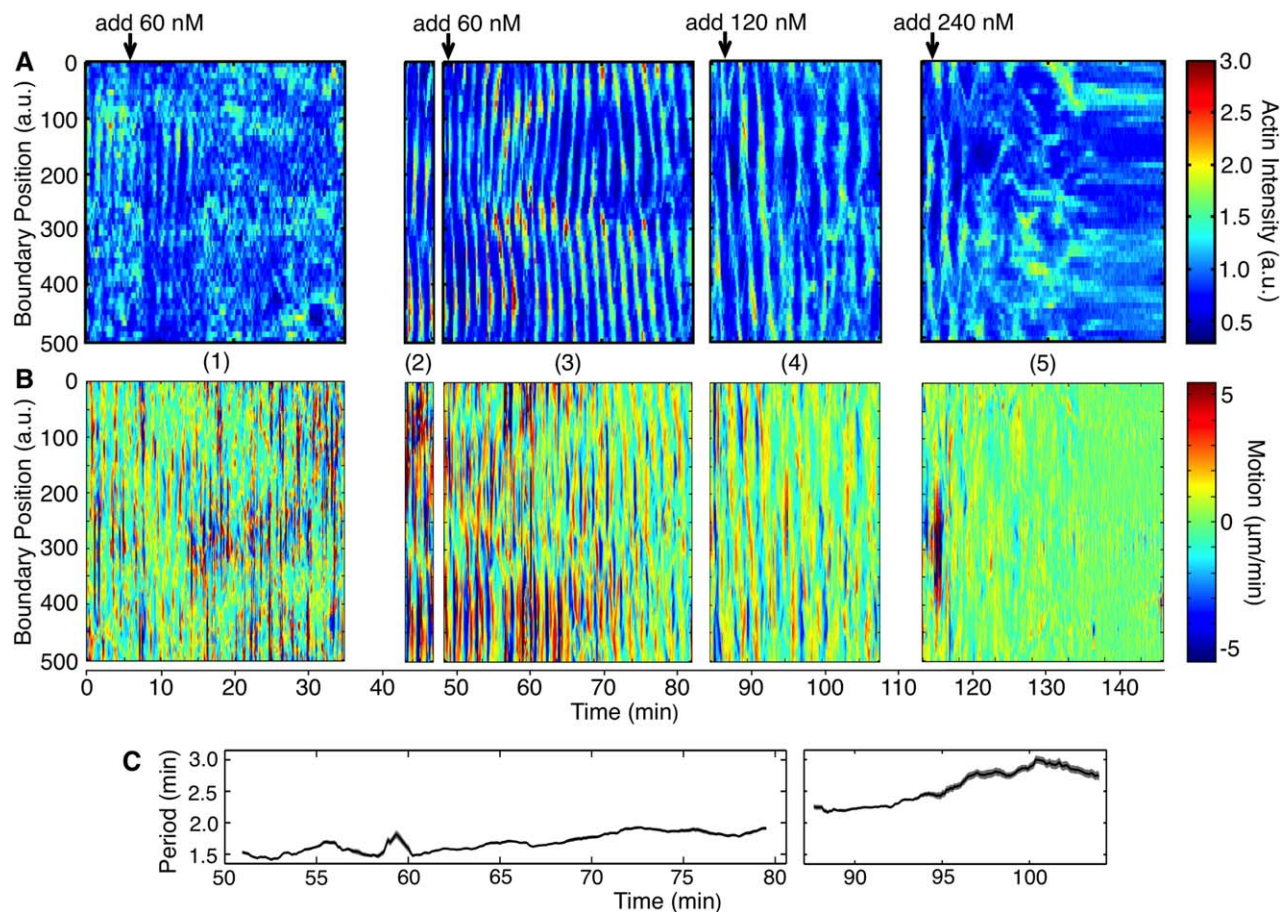
Fig. 8. Effect of Latrunculin treatment on periodically protruding cells. The kymographs of actin fluorescence intensity (**A**) and boundary motion (**B**) of a Latrunculin treated cell. Arrows indicate the times and doses of latrunculin treatment. Note that the experiment had five different episodes with time intervals in between; these episodes correspond to those representative segments shown on Supporting Information Movie 7. (**C**) The period of cell oscillation as a function of time in the interval between 50 and 110 min from the beginning of experiment. The period is defined as the time it takes the cortical actin wave to traverse the cell periphery once. [Color figure can be viewed in the online issue, which is available at wileyonlinelibrary.com.]

2010; Blanchoin et al., 2014). What is remarkable about the periodic protrusive phenotype is the degree to which changes in the local protrusions, cell shape, and actin fluorescence intensity are repeated from cycle to cycle even though they vary strongly within the wave that travels along the boundary. This observation of spatial heterogeneity combined with time periodicity indicates that the medium supporting the wave is spatially inhomogeneous. The fact that the heterogeneity persists over minutes to hours, much longer than the characteristic diffusion time of soluble or membrane bound factors, strongly suggests that the spatially inhomogeneous medium that supports the wave is the cortex itself. The additional fact that the wave can so dramatically yet transiently alter local cell morphology indicates that it does not irreversibly change the cortex architecture. This fact distinguishes compression/dilation waves from actin polymerization waves, which have been shown to alter the structure of the actin network [Gerisch et al., 2011]. The reversible process of cortex compression and dilation sustains highly periodic waves for hours,

whereas actin polymerization waves have short lifetimes and stochastic initiation times and trajectories. Compression/dilation waves and actin polymerization waves also differ in the role played by myosin II. Unlike compression/dilation waves which are inhibited by blebbistatin treatment [Kapustina et al., 2013], actin polymerization waves are not myosin II dependent [Bretschneider et al., 2009].

The temporal interrelationships of the four metrics we analyzed (boundary radius and motion, and actin and plasma membrane intensity) support the qualitative model proposed in Fig. 1 (right panel) of a compression/dilation wave. We found that the actin cortex and plasma membrane intensities are highly correlated everywhere along the boundary and along the wave, consistent with the folding and unfolding of actin cortex and linked plasma membrane as sketched in Fig. 1. Furthermore, the actin intensity peak is preceded by a decrease in cell radius and followed by a rapid outwards boundary motion, consistent with contractile compression that is released after the wave passes through to permit protrusion. Our analysis also sheds light

on the spatial distribution of myosin II, which is thought to be the driver of compression: myosin II is highly correlated with actin density but its signal may be slightly delayed with respect to actin, suggesting that myosin activity could be enhanced by the folded cortex, though there are other possible explanations for the observed time delay as described above.

In examining the boundary motion of periodically protruding cells, we found not only a wave of outwards boundary motion that temporally follows the peak in actin intensity, but also smaller counter-propagating waves (Fig. 7). These counter-propagating waves are also observed as fiduciary features in the images, and appear as "refractions" of the main traveling wave. This can be explained with the qualitative model of a wave traveling through a heterogeneous medium: When a wave travels through a heterogeneous medium, it can encounter rapid changes in the material properties on scales smaller than the wavelength. When any type of wave encounters a sudden change in material properties, it refracts, meaning that part of the wave continues to travel forward and part of the wave is reflected and travels backward. While this refraction is well known for light or sound encountering sharp interfaces, refraction also occurs in a heterogeneous medium. This qualitative explanation for the backward traveling waves implies a long persistence time of the spatial heterogeneity of the medium, since we find refraction events at roughly the same location along the boundary in each cycle over several periods.

Finally, our qualitative model of a spatially heterogeneous excitable medium supporting the compression/dilation wave is consistent with observations that the period of the wave varies from cell to cell. We explore which parameters may drive this variation by sequestering actin monomers via latrunculin treatment. We find that reducing the pool of actin monomers via latrunculin has a twofold effect. For cells that do not naturally exhibit cortex waves, it can trigger the onset of waves. In low concentrations, it can enhance the speed of protrusions for already oscillating cells. In all cells that exhibit cortex waves, further reducing the amount of actin monomer slows down the waves in a spatially heterogeneous way which can lead to intermittent oscillations and changes in wave direction and, in the limit of high latrunculin concentrations, cessation of traveling waves.

The biphasic change in wave behavior in response to latrunculin treatment suggests that there are two or more mechanisms that compete with one another as the latrunculin concentration is varied. For example, if the traveling wave is analogous to a simple harmonic oscillator, we might expect that the frequency of the wave would decrease as the cortex softens with latrunculin treatment resulting in a decrease in traveling wave velocity. On the other hand, we know that compression/dilation waves are myosin dependent via the Rho/ROCK pathway and so we might expect it to be more difficult for myosin to wrinkle a cortex com-

posed of long actin filaments than one composed of actin filaments shortened by latrunculin treatment. In this case, wave velocity might be expected to increase after latrunculin treatment. If both of these mechanisms were operative, we might expect the biphasic response we observe as a function of latrunculin dose. There are a number of more sophisticated mechanisms that involve actin network structure and myosin contractility, as reviewed here [Ryan et al., 2012; Allard and Mogilner, 2013].

Overall, our quantification of highly reproducible dynamics, and our measurements of how such dynamics change under perturbation have yielded new benchmarks and led to the discovery of backward directed waves as a previously unrecognized aspect of the cortex compression/dilation waves. Quantification allows us to take full advantage of the stereotypical nature of the waves: since we can predict the protrusion dynamics, actin dynamics and myosin dynamics with great accuracy, we can determine the effect of drugs and other perturbations on the key cell mechanical elements and their dynamic operation with unprecedented detail. We anticipate that the quantification of boundary dynamics will lead to insights in other cell motility contexts in which periodicity is not necessarily as overt as was demonstrated here.

Materials and Methods

Cell Culture and Transfection

CHO cells stably expressing Lifeact-GFP (the small 17-amino-acid peptide, Lifeact, fused to green fluorescent protein, GFP) and expressing myosin-RFP (myosin fused to red fluorescent protein, RFP) were obtained from James Bear's laboratory (UNC-Chapel Hill). Transfected CHO cells were grown in medium containing 10% FBS (Biowhittaker Lonza, Basel, Switzerland) and 4 mM L-glutamine (Gibco, Invitrogen, Carlsbad, CA) in DMEM/F12 (Gibco) for 2 days to confluency and trypsinized with 1x trypsin-EDTA (Gibco) for 3 min. The supernatant was then spun down at <1000 RPM and the cells were resuspended in 5 mL of media. Nearly 1 mL of this suspension was then added to 35 mm Mat Tek glass bottom dishes (Mat Tek corporation, Ashland, MA), along with an additional 1.5 mL of media. Colchicine, 0.2 μM (Sigma), was added at the time of cell plating unless otherwise noted. Microscope imaging started 30 min after plating. For experiments with Latrunculin A (Enzo Life Sciences) treatment CHO cells were plated on a glass bottom dish 2 h before the experiment.

For the plasma membrane (PM) visualization, we transiently expressed the PM targeting peptide fused to red fluorescent protein (PMT-mRFP) in CHO cells that were stably expressing Lifeact-GFP. PMT-mRFP is a lipid-linked protein that resides almost exclusively on the inner leaflet of the PM. The PMT-mRFP construct was generously provided by Ichiro Maruyama [Liu et al., 2007]. CHO cells

were transiently transfected with PMT-mRFP using Lipofectamine Plus (Invitrogen) and images were taken 24–48 h after transfection.

Microscope Imaging

Optical images were acquired using an Olympus FluoView 1000 laser scanning confocal microscope with an environmental chamber. Images were captured in sequential line scanning mode with 60x and 100x oil immersion objectives. Images with increased time resolution were obtained using a Nipkow-type spinning disk confocal scan head (Yokogawa CSU-10) with a $60\times$ 1.45 NA objective mounted on an Olympus IX-83 stand and recorded using an Andor EMCCD camera.

Measuring and Tracking the Cell Boundary

The cell boundary was extracted from each image using a modified snake algorithm [Xu and Prince, 1998] (as described previously [Driscoll et al., 2014]). The boundary in each frame is mathematically represented as the positions of a sequence of 500 equidistant points along that boundary. Boundary points are labeled increasing sequentially in the counter-clockwise direction and boundary point 0 is defined as the boundary point closest to 0 degrees relative to the boundary centroid. Boundary points were tracked from frame to frame by associating same-labeled boundary points in successive frames (see [Driscoll et al., 2011] for a comparison of boundary point tracking methods). At each boundary point, boundary motion was calculated as previously described [Driscoll et al., 2011].

Measuring Fluorescence Intensity

We measured fluorescence intensity along the boundary by tiling an outer shell of the area occupied by the cell with quadrilaterals and measuring the average intensity inside each quadrilateral (Fig. 4A). (The tiling is motivated by that found in [Machacek et al., 2009]. The outer ring of the shell was defined as the cell boundary. The inner ring was found by morphologically eroding the cell boundary by ~20 pixels, so that each point on the inner ring is ~20 pixels from the cell boundary. Every 4th or 5th point on the cell boundary was next connected to a point on the inner ring. We connected the points on the outer ring to the points on the inner ring by choosing the 1:1 mapping that minimized the sum of the distances between connected points and that did not allow connections to cross. For each quadrilateral tile, we then measured the average intensity of the pixels that were entirely inside the tile.

To compare intensities between different fluorescence reporters, we corrected the intensities for photobleaching. In each frame, the mean intensity averaged across the tiles was found. Mean GFP intensities were fit to a single exponential decay in time, whereas mean RFP intensities were fit to a sum of two exponential decays. The intensity in each tile was then finally normalized by the fit.

Correlation Analysis

For auto and cross-correlations, the temporal correlation, ρ, of measures X and Y at each boundary point was calculated as $\rho_{XY}(m) = E[(X_n - \mu_X)(Y_{n+m} - \mu_Y)]/(\sigma_x \sigma_y)$, where m is the time lag, μ is the mean of the measure at the boundary point, σ is the standard deviation of the measure at the boundary point, and n is the time, which the expectation value is measured across. For the protrusive and retractive motion measures, the mean of the measure was not subtracted.

Measuring the Wave Period

The wave period at every frame was estimated from the fluorescence intensity of actin measured at the cell boundary. The actin intensity was measured as described above and was corrected for photobleaching. At each boundary point and frame, the period was then measured from a temporal autocorrelation over an adaptive window size. The window chosen was symmetric about the frame under calculation. The autocorrelation was interpolated using a cubic spline with a step size of 1/20 of the time between frames. From the spline fit, the time delay of the first peak in the autocorrelation was calculated as the wave period at that boundary point and time and the magnitude of that peak was calculated as the period strength. The period at each time was then found as the period averaged across boundary points and weighted by period strength. Its error was calculated as the standard error of the weighted mean. For the first frame in each movie, the autocorrelation window size was set by the user, but subsequent frames use the period calculated in the previous frame times 1.3 as the window size.

Acknowledgments

References

Allard J, Mogilner A. 2013. Traveling waves in actin dynamics and cell motility. Curr Opin Cell Biol 25:107–115.

Blanchoin L, Boujemaa-Paterski R, Sykes C, Plastino J. 2014. Actin dynamics, architecture, and mechanics in cell motility. Physiol Rev 94:235–263.

Bretschneider T, Anderson K, Ecke M, Müller-Taubenberger A, Schroth-Diez B, Ishikawa-Ankerhold HC, Gerisch G. 2009. The

three-dimensional dynamics of actin waves, a model of cytoskeletal self-organization. Biophys J 96:2888–2900.

Cai Y, Rossier O, Gauthier NC, Biais N, Fardin MA, Zhang X, Miller LW, Ladoux B, Cornish VW, Sheetz MP. 2010. Cytoskeletal coherence requires myosin-IIA contractility. J Cell Sci 123:413–423.

Costigliola N, Kapustina M, Weinreb GE, Monteith A, Rajfur Z, Jacobson K, Elston TC. 2010. RhoA regulates calcium independent periodic contractions of the cell cortex. Biophys J 99:1053–1063.

Courson DS, Rock RS. 2010. Actin cross-link assembly and disassembly mechanics for α-actinin and fascin. J Biol Chem 285:26350–26357.

Driscoll MK, Fourkas JT, Losert W. 2011. Local and global measures of shape dynamics. Phys Biol 8:055001.

Driscoll MK, Sun X, Guven C, Fourkas JT, Losert W. 2014. Cellular contact guidance through dynamic sensing of nanotopography. ACS Nano 8:3546–3555.

Friedl P, Wolf K. 2010. Plasticity of cell migration: A multiscale tuning model. J Cell Biol 188:11–19.

Gardel ML, Shin JH, MacKintosh FC, Mahadevan L, Matsudaira P, Weitz DA. 2004. Elastic behavior of cross-linked and bundled actin networks. Science 304:1301–1305.

Gerisch G, Ecke M, Wischnewski D, Schroth-Diez B. 2011. Different modes of state transitions determine pattern in the phosphatidylinositide-actin system. BMC Cell Biol 12:1–16.

Kapustina M, Elston TC, Jacobson K. 2013. Compression and dilation of the membrane-cortex layer generates rapid changes in cell shape. J Cell Biol 200:95–108.

Kasza KE, Zallen JA. 2011. Dynamics and regulation of contractile actin–myosin networks in morphogenesis. Curr Opin Cell Biol 23:30–38.

Kasza KE, Nakamura F, Hu S, Kollmannsberger P, Bonakdar N, Fabry B, Stossel TP, Wang N, Weitz DA. 2009. Filamin A is essential for active cell stiffening but not passive stiffening under external force. Biophys J 96:4326–4335.

Keren K, Pincus Z, Allen GM, Barnhart EL, Marriott G, Mogilner A, Theriot JA. 2008. Mechanism of shape determination in motile cells. Nature 453:475–480.

Liu P, Sudhaharan T, Koh RML, Hwang LC, Ahmed S, Maruyama IN, Wohland T. 2007. Investigation of the dimerization of proteins from the epidermal growth factor receptor family by single wavelength fluorescence cross-correlation spectroscopy. Biophys J 93:684–698.

Machacek M, Hodgson L, Welch C, Elliott H, Pertz O, Nalbant P, Abell A, Johnson GL, Hahn KM, Danuser G. 2009. Coordination of Rho GTPase activities during cell protrusion. Nature 461:99–103.

Maciver SK. 1996. Myosin II function in non-muscle cells. Bioessays 18:179–182.

Mitchison TJ, Cramer LP. 1996. Actin-based cell motility and cell locomotion. Cell 84:371–379.

Pletjushkina OJ, Rajfur Z, Pomorski P, Oliver TN, Vasiliev JM, Jacobson KA. 2001. Induction of cortical oscillations in spreading cells by depolymerization of microtubules. Cell Motil Cytoskeleton 48:235–244.

Prass M, Jacobson K, Mogilner A, Radmacher M. 2006. Direct measurement of the lamellipodial protrusive force in a migrating cell. J Cell Biol 174:767–772.

Revenu C, Athman R, Robine S, Louvard D. 2004. The co-workers of actin filaments: From cell structures to signals. Nat Rev Mol Cell Biol 5:635–646.

Riedl J, Crevenna AH, Kessenbrock K, Yu JH, Neukirchen D, Bista M, Bradke F, Jenne D, Holak TA, Werb Z, Sixt M, Wedlich-Soldner R. 2008. Lifeact: A versatile marker to visualize F-actin. Nat Methods 5:605–607.

Rottner K, Stradal TEB. 2011. Actin dynamics and turnover in cell motility. Curr Opin Cell Biol 23:569–578.

Ryan GL, Watanabe N, Vavylonis D. 2012. A review of models of fluctuating protrusion and retraction patterns at the leading edge of motile cells. Cytoskeleton 69:195–206.

Tseng Y, Fedorov E, McCaffery JM, Almo SC, Wirtz D. 2001. Micromechanics and ultrastructure of actin filament networks cross-linked by human fascin: A comparison with α-actinin. J Mol Biol 310:351–366.

Xu C, Prince JL. 1998. Snakes, shapes, and gradient vector flow. Image Process IEEE Trans 7:359–369.